



Cite this: DOI: 10.1039/d5ta08126b

## From anion-centric to cation-enabled energetics: planar tetrazine frameworks with enhanced stability

Jatinder Singh, <sup>a</sup> Richard J. Staples <sup>b</sup> and Jean'ne M. Shreeve <sup>\*a</sup>

Nitrogen-rich heterocycles represent a fertile ground for novel reactions and unusual molecular conversions, which not only advance fundamental heterocyclic chemistry but also enable the design of next-generation energetic materials. Owing to their high energy densities and clean decomposition into environmentally benign nitrogen gas, such frameworks are of growing importance in energy and environmental science. We report a new class of tetrazine-derived cationic and zwitterionic frameworks that enable thermally robust, high-performance energetic salts suitable for advanced propellant and energetic applications. Unlike conventional anion-centric approaches, our design focuses on planar, high-nitrogen tetrazine cations that promote  $\pi$ - $\pi$  stacking interactions, hydrogen bond networks, and compact layer-like packing. These structural characteristics yield thermal decomposition onsets of 163–320 °C, densities of 1.61–1.80 g cm<sup>-3</sup>, and calculated detonation velocities of 7866–9292 m s<sup>-1</sup> with corresponding detonation pressures of 21–34 GPa. Our zwitterionic tetrazine highlights how cation engineering and zwitterionic design together expand the scope of tetrazine chemistry toward thermally robust energetic materials. This work expands the scope of tetrazine chemistry and highlights the utility of planar high-nitrogen frameworks in the design of stable energetic materials.

Received 4th October 2025  
Accepted 18th December 2025

DOI: 10.1039/d5ta08126b  
[rsc.li/materials-a](http://rsc.li/materials-a)

## 1 Introduction

High-nitrogen energetic materials are valued for their ability to couple strong detonation performance with environmentally benign decomposition into nitrogen gas.<sup>1–5</sup> Incorporation of high-energy explosophores into nitrogen-rich heterocycles has therefore become a major design strategy, as these frameworks enhance energy density while allowing structural diversification through selective functionalization (Fig. 1A).<sup>6–10</sup> However, this approach often introduces a central drawback: compounds bearing strongly energetic substituents typically suffer from poor thermal stability and increased sensitivity to external stimuli such as impact and friction.<sup>11–15</sup> Balancing energy density with safety thus remains a fundamental challenge in practical energetic-material design.<sup>16–20</sup>

Energetic salts provide a promising pathway to address this issue. By deprotonating acidic heterocycles or introducing acidic energetic substituents, salts can be generated *via* pairing with suitable cations or anions (Fig. 1B).<sup>21,22</sup> Their ionic nature fosters dense crystal lattices stabilized by hydrogen bonding and other non-covalent interactions, which result in reduced mechanical sensitivity while retaining high energy content (Fig.

1C).<sup>23,24</sup> Despite these advantages, progress in salt design has been strongly skewed toward anions. Nitro-, nitramino-, and azido-substituted heterocycles dominate the literature whereas energetic cations are comparatively rare and structurally simple, typically limited to ammonium, hydroxylammonium, guanidinium, or small amino/alkyl-substituted systems. This imbalance highlights the urgent need for innovative cation-design strategies.<sup>25–30</sup>

Within the family of nitrogen-rich heterocycles, tetrazines have emerged as particularly compelling scaffolds due to their exceptional nitrogen content, synthetic versatility, and ability to host diverse functional groups.<sup>31–35</sup> The 1,2,4,5-tetrazine ring has been exploited to produce energetic salts with tunable properties, fused heterocyclic frameworks with enhanced aromatic stabilization, and coordination-driven polymers where metal-ligand interactions impart additional stability. A defining feature of planar tetrazine frameworks is their strong  $\pi$ -delocalization, which contributes both to aromatic stabilization and efficient crystal packing. This combination increases density and detonation performance while simultaneously improving thermal stability—critical attributes for safe handling and long-term storage.<sup>36–40</sup>

Recent studies have also revealed that substitution on the tetrazine ring can induce unusual chemical transformations, ranging from nucleophilic substitution cascades to acid-mediated nitration and nitramination. Such reactivity broadens the scope of accessible derivatives, including cationic,

<sup>a</sup>Department of Chemistry, University of Idaho, Moscow 83844-2343, ID, USA. E-mail: [jshreeve@uidaho.edu](mailto:jshreeve@uidaho.edu); Fax: (+1) 208-885-5173

<sup>b</sup>Department of Chemistry, Michigan State University, East Lansing 48824, Michigan, USA



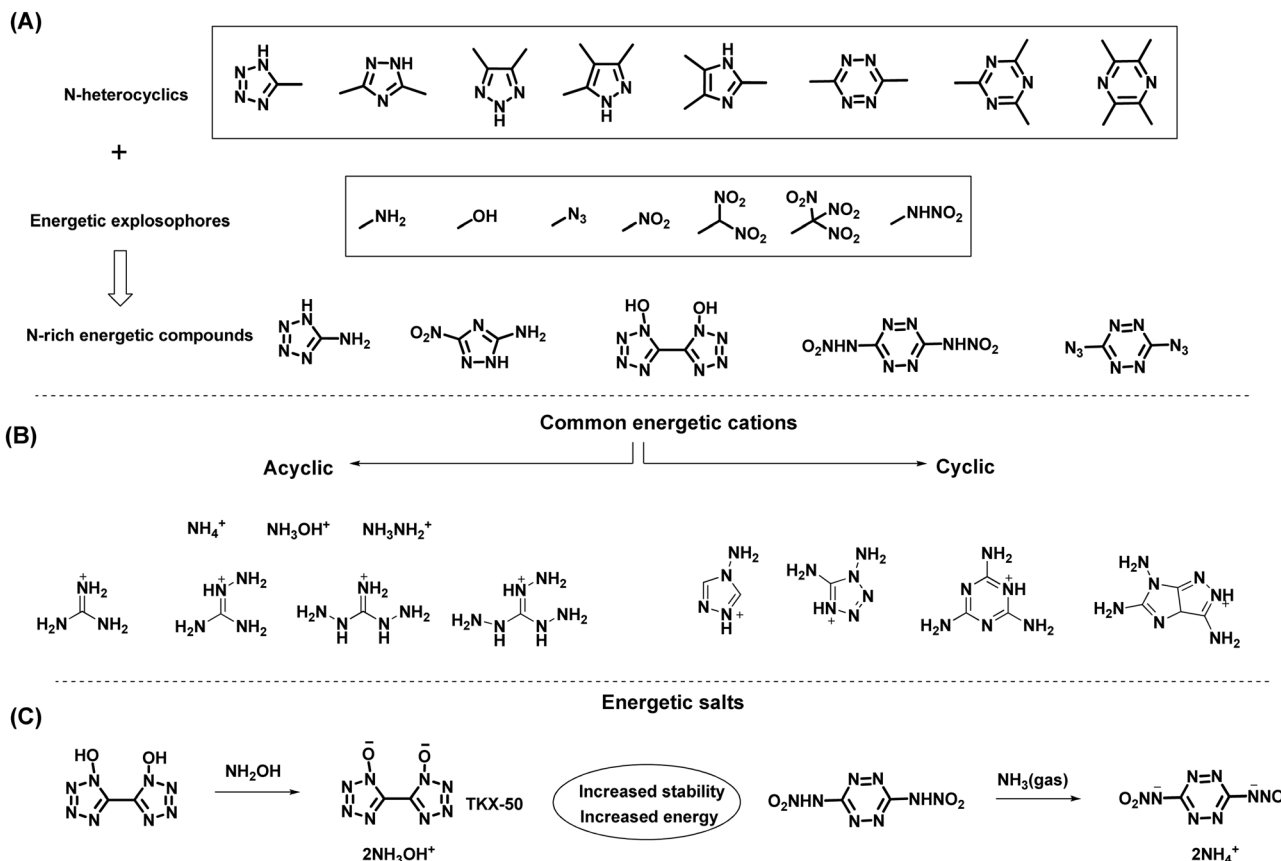


Fig. 1 Production of new energetic materials. (A) N-heterocyclics, energetic explosives and N-rich compounds. (B) Commonly used energetic cations. (C) Energetic salts formation.

fused, or coordination-stabilized variants, some of which achieve a rare balance of high energy output with moderated sensitivities. These advances underscore the adaptability of the tetrazine core and highlight its promise as a platform for rational energetic-cation design. In this context, the present work explores the synthesis and characterization of tetrazine-based cations that integrate high nitrogen content, planar frameworks, and excellent thermal stability (Fig. 2). By shifting attention from anion-focused strategies to cation engineering, we aim to advance the design of high-performance, safer energetic salts.

## 2 Results and discussion

### 2.1 Synthesis

3,6-Bis(3,5-dimethyl-1*H*-pyrazol-1-yl)-1,2,4,5-tetrazine (**P1**), 6-(3,5-dimethyl-1*H*-pyrazol-1-yl)-1,2,4,5-tetrazin-3-amine (**P2**), and *N*-(6-(3,5-dimethyl-1*H*-pyrazol-1-yl)-1,2,4,5-tetrazin-3-yl) nitramide (**P3**) were synthesized following established literature procedures.<sup>41,42</sup> The reaction of **P1** and **P2** with guanidine in methanol results in the formation of 2,2'-(1,2,4,5-tetrazine-3,6-diyil)diguanidine (**L1**) and 2-(6-amino-1,2,4,5-tetrazin-3-yl) guanidine (**L2**), respectively (Scheme 1A). The reaction of **L1** and **L2** with hydrochloric acid gives chloride salts **L1-2Cl**, and **L2-Cl**, respectively.

The sodium or potassium or ammonium salts (**A1–A5**) were synthesized following established literature procedures (Scheme 1B).<sup>43–48</sup> The sodium or potassium or ammonium salts of compounds **A1–A5** were reacted with the hydrochlorides (**L1-2Cl** and **L2-Cl**) in aqueous solution to obtain assembled products (Scheme 1B). While the synthesis of **L1** itself has been described earlier by our group, the salts and ionic derivatives presented here, which differ in counter-ion identity and solid-state packing, are unprecedented. These new salts exhibit distinct crystal-packing motifs, thermal behaviour, and mechanical-sensitivity profiles, and therefore materially expand the scope and application potential of the **L1** scaffold. The reaction of **P3** with guanidine in methanol results in the formation of compound **1**, which was neutralized with aqueous HCl to give the zwitterionic compound **2** (Scheme 1C).

### 2.2 Characterization

**2.2.1 NMR spectroscopy.** All new compounds were analyzed and characterized through <sup>1</sup>H, <sup>13</sup>C NMR spectroscopy (ESI). In the <sup>13</sup>C NMR spectrum of **L1**, two carbon peaks were observed at 162.6 ppm and 158.0 ppm, respectively. The unsymmetric **L2** shows carbon peaks at 164.4, 160.1, and 157.7 ppm, respectively. Upon salt formation with acids, the two carbon peaks in **L1** were shifted upfield to 158.5 ppm and 154.4 ppm, respectively. Similarly, for **L2**, the three carbon



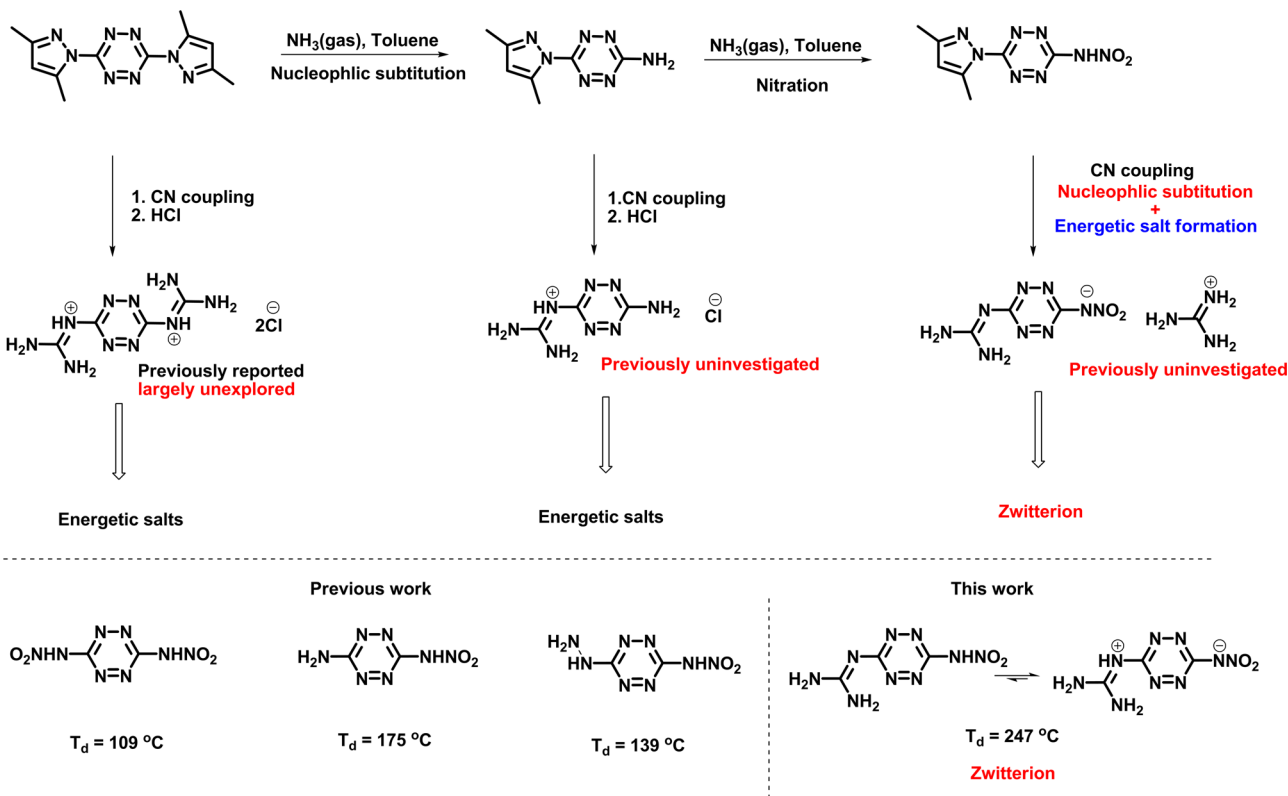


Fig. 2 Previous work and present work.

peaks were shifted upfield to 162.9, 156.1, 154.9 ppm, respectively. Given the high nitrogen content of all the compounds, the  $^{14}\text{N}$  and  $^{15}\text{N}$  spectra of selected compounds were recorded (ESI). The  $^{15}\text{N}$  NMR spectra of **L1**, **L2**, and compound 2 are shown in Fig. 3.

The  $^{14}\text{N}$  NMR spectrum of precursor **P3** shows the characteristic nitramine  $\text{N}-\text{NO}_2$  resonance at  $-34.5$  ppm for the neutral molecule (Fig. 3D). In contrast, upon deprotonation the corresponding nitramine nitrogen in compound **1** (guanidinium salt) shifts markedly upfield to  $-12.2$  ppm (Fig. 3E), and a similar shift is observed in the zwitterionic compound **2** at  $-11.8$  ppm (Fig. 3F). This substantial upfield migration of the nitramine signal clearly indicates that, in the zwitterionic structure, the nitramine moiety exists predominantly in its anionic (deprotonated) form.

**2.2.2 Crystal structure.** Single crystals of compound **L2** suitable for X-ray analysis were obtained by slow evaporation from DMSO. It crystallizes in a monoclinic ( $P2_1/c$ ) space group (Fig. 4A). The crystal structure supports the structure of **L2**, resulting in the molecular formula  $\text{C}_3\text{H}_6\text{N}_8$ , with a calculated crystal density of  $1.677 \text{ g cm}^{-3}$  at  $100 \text{ K}$ .

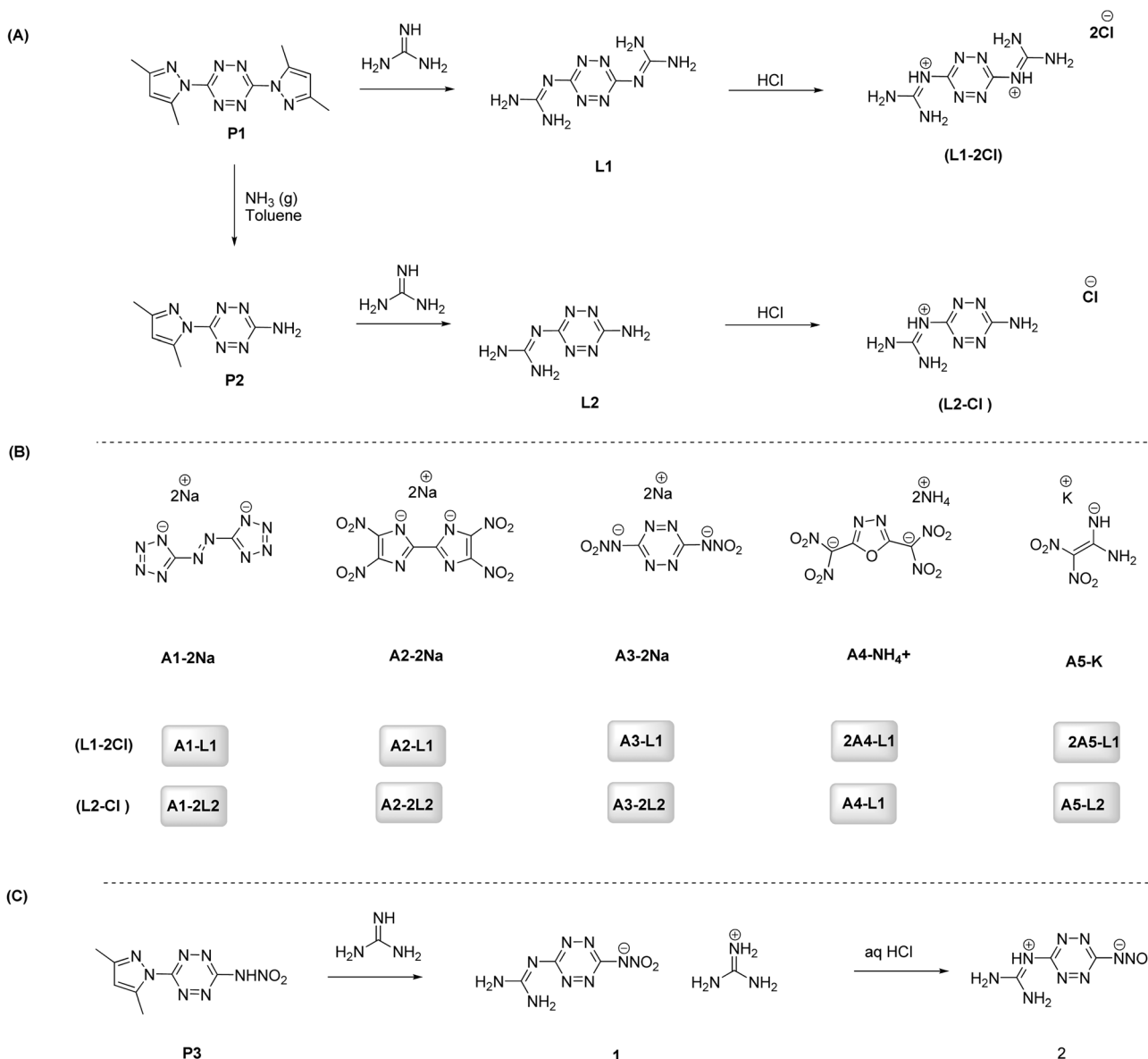
Single crystals of compound **A1-L1** suitable for X-ray analysis were obtained by slow evaporation from DMSO. It crystallizes in a monoclinic ( $P2_1/n$ ) space group (Fig. 5A). The crystal structure supports the presence of anion and cation in  $1:1$  ratio, resulting in the molecular formula  $\text{C}_6\text{H}_{10}\text{N}_{20}$ , with a calculated crystal density of  $1.715 \text{ g cm}^{-3}$  at  $100 \text{ K}$ .

In Fig. 5B the planar arrangement of both the anion and cation species is seen. Compound **A1-L1** has planar stacking with layer spacing of  $3.14 \text{ \AA}$ , which is lower than the typical  $3.65\text{--}4.00 \text{ \AA}$  observed in aromatic  $\pi\text{-}\pi$  interactions. The interlayer spacing suggests that there may be strong  $\pi\text{-}\pi$  interactions between the molecules (Fig. 5C). This enhanced stacking contributes to the compact packing and may explain the relatively high density of the crystal. Single crystals of compound **A3-2L2** suitable for X-ray analysis were obtained by slow evaporation from DMSO. It crystallizes in a monoclinic ( $I2/a$ ) space group (Fig. 6). The crystal structure supports the presence of anion and cation in  $1:2$  ratio, resulting in the molecular formula  $\text{C}_8\text{H}_{14}\text{N}_{24}\text{O}_4$  with a density of  $1.811 \text{ g cm}^{-3}$  at  $100 \text{ K}$ . Each dinitramide anion is sandwiched between **L2** cations through  $\pi\text{-philic}$  molecular recognition interactions.

### 2.3 Physicochemical properties

High thermal stability is crucial for useful energetic materials. Thermal characteristics were determined using differential scanning calorimetry (DSC) analysis. At  $5 \text{ }^{\circ}\text{C min}^{-1}$ , the decompositions of **L1** and **L2** occur at  $274 \text{ }^{\circ}\text{C}$  (onset) and  $265 \text{ }^{\circ}\text{C}$  (onset), respectively. The energetic salts exhibit decomposition temperatures in the range of  $163 \text{ }^{\circ}\text{C}$  to  $320 \text{ }^{\circ}\text{C}$  (onset), respectively. To study structure–property relationships, an in-depth exploration of weak interactions was conducted *via* Hirshfeld surface and 2D fingerprint analyses (Fig. 7).<sup>49,50</sup> The red regions on the Hirshfeld surfaces indicate interactions between





Scheme 1 (A) Synthesis of 2,2'-(1,2,4,5-tetrazine-3,6-diyl)diguanidine (L1) and 2-(6-amino-1,2,4,5-tetrazin-3-yl)guanidine (L2). (B) Sodium or potassium salts of compounds A1–A5 and assembled products. (C) Synthesis of compound 2.

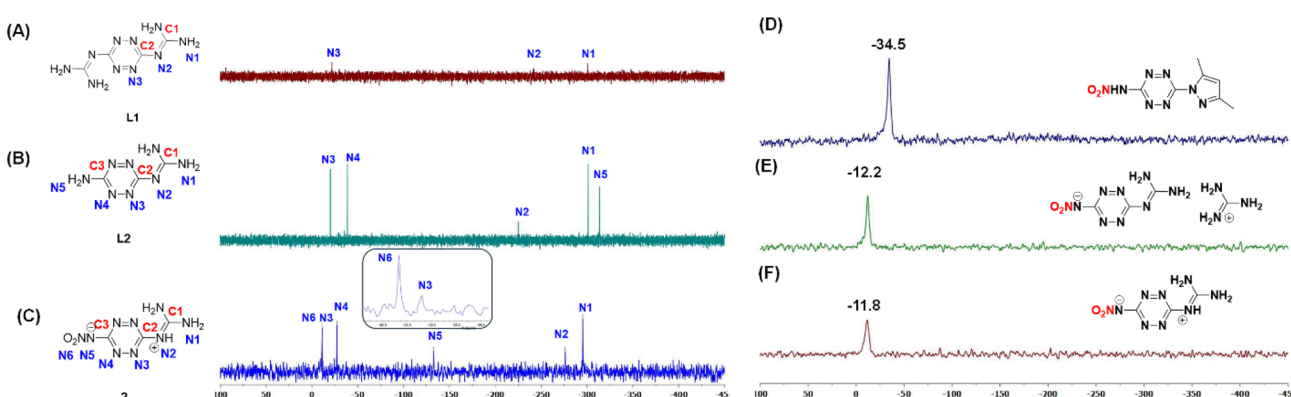


Fig. 3 <sup>15</sup>N NMR of (A) L1. (B) L2. (C) 2. <sup>14</sup>N NMR of (D) P3. (E) 1. (F) 2.

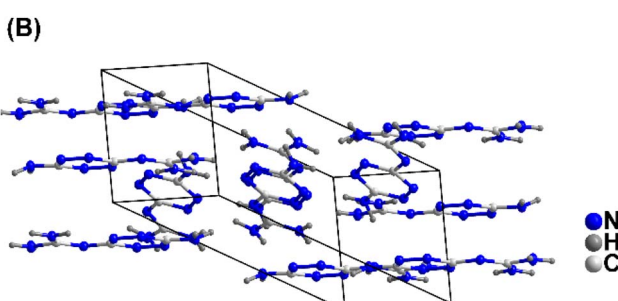
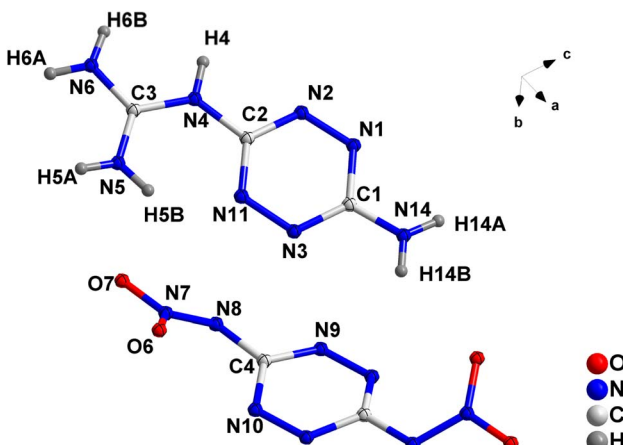
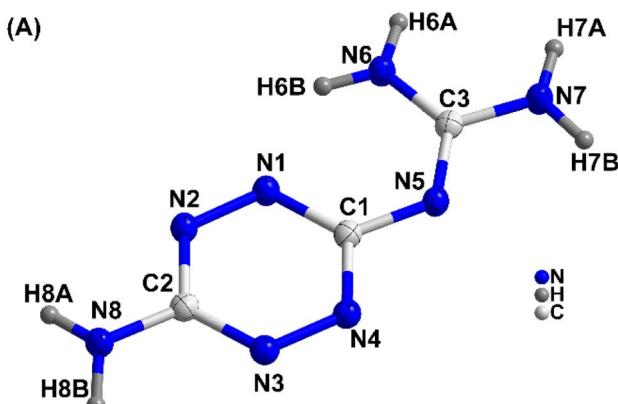


Fig. 4 (A) Labeling scheme for L2 (thermal ellipsoid at 50%). (B) Packing diagram of L2.

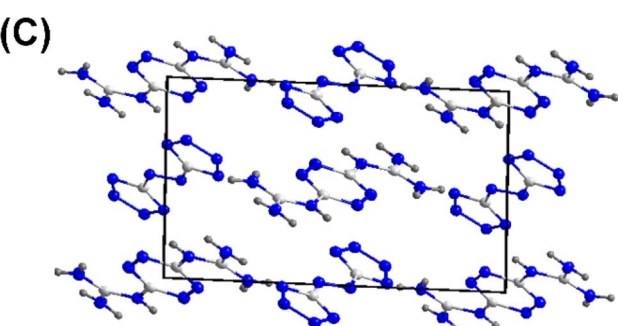
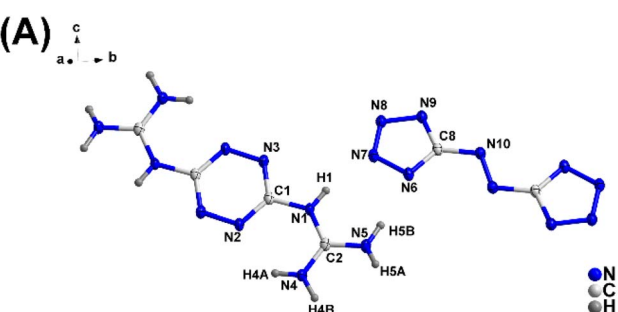


Fig. 5 (A) Labeling scheme for A1-L1 (thermal ellipsoid at 50%). (B) Planar structure of A1-L1. (C) Packing diagram of A1-L1.

Fig. 6 Labeling scheme for A3-2L2 (thermal ellipsoid at 50%).

neighboring molecules. The  $\pi$ - $\pi$  interactions aroused by stacking of the dianion and two mono cations are visualized by plotting non-covalent interactions plots. In compound A1-L1, the nitrogen atoms of the anion form strong hydrogen bonds with the surrounding cations, with bond lengths ranging from 2.00 Å to 2.21 Å (Fig. 7M).

The total amount of H-bond interactions, N-H $\cdots$ N, is 61.6% (Fig. 7J and M). The percentage of N $\cdots$ N and N $\cdots$ C interactions is 27.3%, which indicates the presence of  $\pi$ - $\pi$  stacking between the rings. The larger value of these stabilizing interactions enhances molecular stability and insensitivity of A1-L1. For compound A3-2L2, the four O atoms from two nitroamino groups are fixed by H bonds from the surrounding cations, with lengths ranging from 1.91 Å to 2.44 Å (Fig. 7T). The total amount of H-bond interactions, O-H $\cdots$ N and N-H $\cdots$ N, is 62.7% (Fig. 7P and Q). The percentage of N $\cdots$ N and N $\cdots$ C interactions is 21.6%, which indicates the presence of  $\pi$ - $\pi$  stacking between the rings. Compound A3-2L2 also has planar stacking with layer spacing of 3.25 Å (Fig. 7U).

For all compounds, sensitivities to impact and friction were measured by using BAM standard methods<sup>51,52</sup> and are given in Table 1.

These compounds show acceptably low sensitivity towards impact and friction. The sensitivities of compounds A1-L1 and A3-2L2 are further explained from both crystal structure and at the molecular level. They have a layer-like packing pattern in the crystal structure, which when subjected to external stimuli can transform the mechanical energy into relative motion between layers. At the molecular level, sensitivities of materials toward impact are very closely related to their electrostatic potentials (ESPs). The electrostatic potentials of compounds A1-L1 and A3-2L2 were calculated based on the B3LYP/6-311G(d, p) method with optimized structures. ESP minima and maxima for compounds



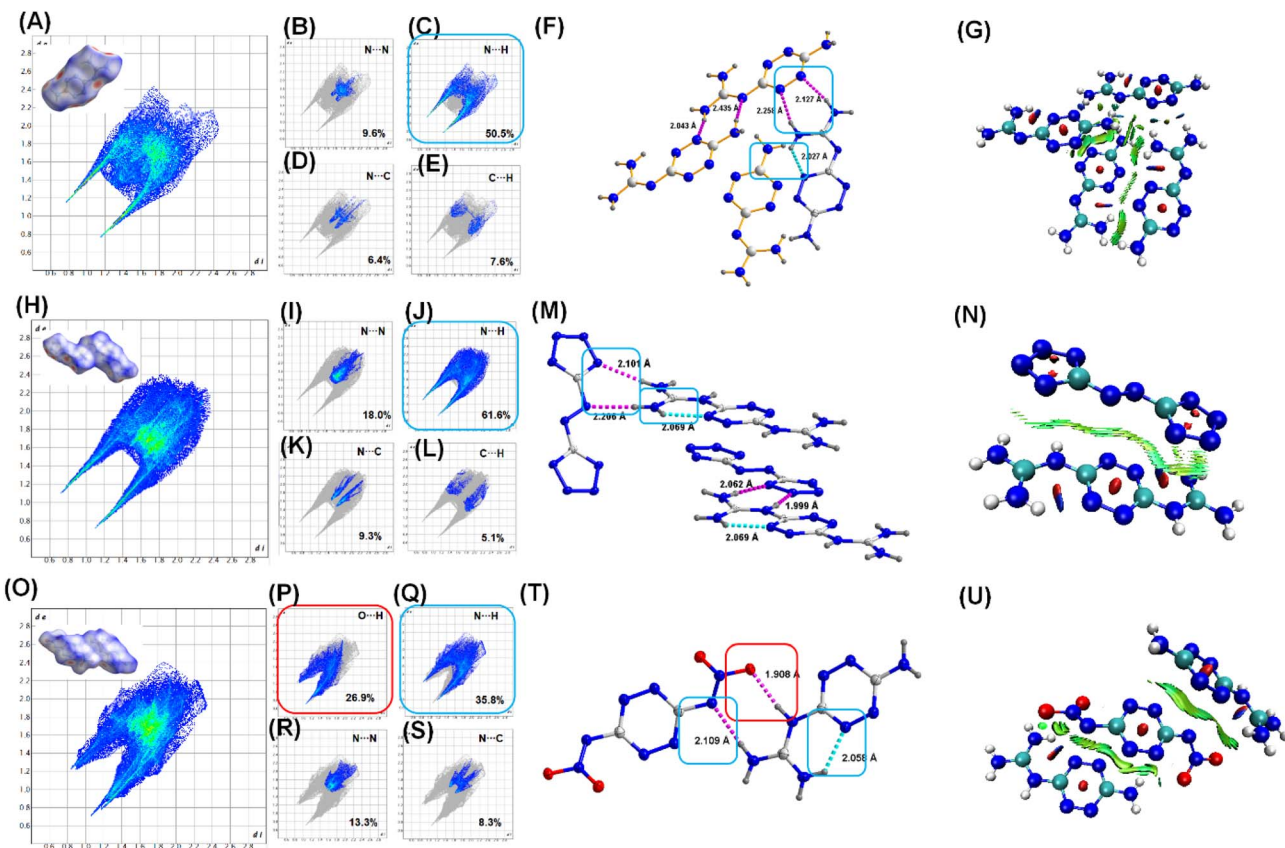


Fig. 7 (A–E) Hirshfeld surface, 2D fingerprint plots of L2. (F) H-bond interaction in L2 (G) NCI plot of L2. (H–L) Hirshfeld surface, 2D fingerprint plots of A1–L1. (M) H-bond interaction in A1–L1 (N) NCI plot of A1–L1. (O–S) Hirshfeld surface, 2D fingerprint plots of A3–2L2. (T) H-bond interaction in A3–2L2 (U) NCI plot of A3–2L2.

A1–L1 and A3–2L2 are  $-78.9$ ,  $-78.4$  kcal mol $^{-1}$  and  $+96.4$ ,  $+90.9$  kcal mol $^{-1}$ , respectively (Fig. 8).

The densities of all compounds were measured using a gas pycnometer at ambient temperature under a helium (He)

atmosphere and range from  $1.61$  g cm $^{-3}$  to  $1.79$  g cm $^{-3}$  (Table 1). The enthalpies of formation of the new compounds were calculated using the isodesmic method with the Gaussian 03 suite of programs<sup>53</sup> giving values for compounds in the range from 0.42 to

Table 1 Physicochemical properties of compounds

	MF <sup>h</sup>	T <sub>d</sub> <sup>a</sup> (°C)	IS <sup>b</sup> (J)	FS <sup>c</sup> (N)	ρ <sup>d</sup> (g cm $^{-3}$ )	ΔH <sub>f</sub> <sup>e</sup> (kJ g $^{-1}$ )	D <sub>v</sub> <sup>f</sup> (m s $^{-1}$ )	P <sup>g</sup> (GPa)
<b>L1</b>	C <sub>4</sub> H <sub>8</sub> N <sub>10</sub>	274	40	360	1.61*	2.59	7866	21.0
<b>L2</b>	C <sub>3</sub> H <sub>6</sub> N <sub>8</sub>	265	40	360	1.62	2.98	8020	22.2
<b>A1–L1</b>	C <sub>6</sub> H <sub>10</sub> N <sub>20</sub>	163	20	240	1.67*	6.18	8970	30.3
<b>A1–2L2</b>	C <sub>8</sub> H <sub>14</sub> N <sub>26</sub>	195	25	360	1.66	3.64	8191	23.7
<b>A2–L1</b>	C <sub>10</sub> H <sub>10</sub> N <sub>18</sub> O <sub>8</sub>	317	25	360	1.74	2.87	8353	28.4
<b>A2–2L2</b>	C <sub>12</sub> H <sub>14</sub> N <sub>24</sub> O <sub>8</sub>	320	30	360	1.75	1.62	7911	23.6
<b>A3–L1</b>	C <sub>6</sub> H <sub>10</sub> N <sub>18</sub> O <sub>4</sub>	216	15	360	1.74	5.25	9292	34.2
<b>A3–2L2</b>	C <sub>8</sub> H <sub>14</sub> N <sub>24</sub> O <sub>4</sub>	256	20	360	1.76*	3.07	8717	28.6
<b>A4–L1</b>	C <sub>8</sub> H <sub>10</sub> N <sub>16</sub> O <sub>9</sub>	186	15	360	1.78	2.65	8804	33.0
<b>A4–2L2</b>	C <sub>10</sub> H <sub>14</sub> N <sub>22</sub> O <sub>9</sub>	222	16	360	1.72	1.35	8015	24.5
<b>2A5–L1</b>	C <sub>8</sub> H <sub>16</sub> N <sub>18</sub> O <sub>8</sub>	200	20	360	1.79	2.46	9036	32.7
<b>A5–L2</b>	C <sub>5</sub> H <sub>10</sub> N <sub>12</sub> O <sub>4</sub>	243	25	360	1.77	3.04	9040	32.2
<b>1</b>	C <sub>4</sub> H <sub>10</sub> N <sub>12</sub> O <sub>2</sub>	263	30	360	1.63	2.13	8220	24.0
<b>2</b>	C <sub>3</sub> H <sub>5</sub> N <sub>9</sub> O <sub>2</sub>	247	10	160	1.80	3.17	8967	31.5
<b>RDX<sup>i</sup></b>	C = H <sub>6</sub> N <sub>6</sub> O <sub>6</sub>	204	7.5/5.6*	120	1.80	0.42	8795	34.9

<sup>a</sup> Temperature (onset at 5 °C min $^{-1}$ ) of decomposition. <sup>b</sup> Sensitivity to impact (IS). <sup>c</sup> Sensitivity to friction (FS). <sup>d</sup> Density at 25 °C using gas pycnometer. <sup>e</sup> Enthalpy of formation (calculated using isodesmic reactions with the Gaussian 03 suite of programs (revision D.01). <sup>f</sup> Velocity (calculated using EXPLO5 version 7.01.01). <sup>g</sup> Pressure (calculated using EXPLO5 version 7.01.01) (calculated using EXPLO5 version 7.01.01).

<sup>h</sup> Molecular formula. <sup>i</sup> Ref. 55. \* $h_{50} = 24$  cm/2.5 kg hammer (ref. 56). \*Calculated crystal density (RT).



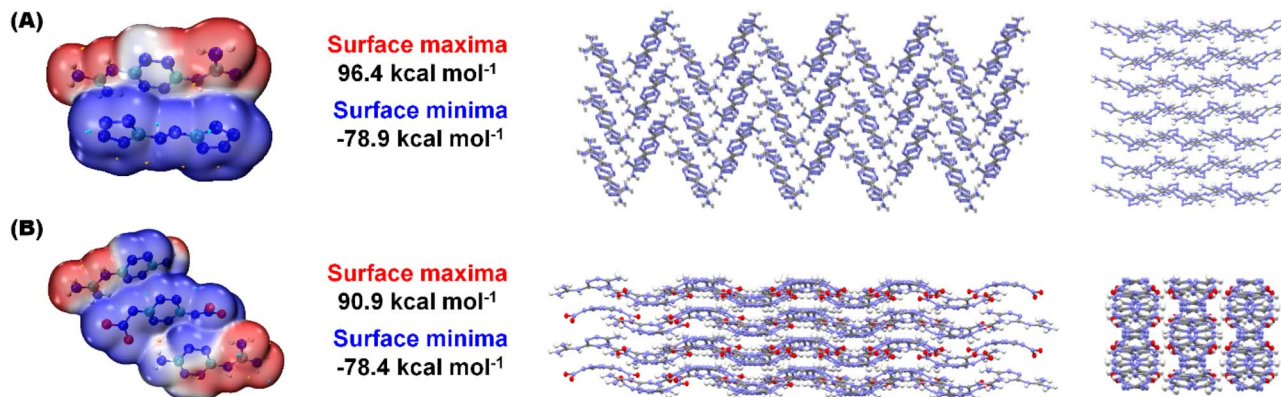


Fig. 8 ESP surfaces and packing diagrams (A) A1-L1 (B) A3-L2.

6.18 kJ g<sup>-1</sup> (Table 1). All compounds have positive enthalpies of formation owing to the presence of multiple N···N bonds. With experimental densities and calculated enthalpies of formation, detonation properties were calculated using EXPLO5 (v7.01.01).<sup>54</sup> The values of calculated detonation velocities and detonation pressures are given in Table 1 and fall between 7866–9292 m s<sup>-1</sup> and 21.0–34.2 GPa, respectively, with **A3-L1** showing the highest calculated detonation velocity and the highest pressure.

In addition to their favourable thermal and energetic characteristics, the poor solubility of these salts should be emphasized as a structural consequence of their molecular design. The relatively large size and high nitrogen content of the cations increase polarity and reduce compatibility with common organic solvents (Fig. 9A). At the same time, extensive intramolecular

hydrogen bonding and  $\pi$ – $\pi$  stacking interactions promote compact crystal packing, which further limits solvent penetration. These combined factors lead to materials that are markedly less soluble than many conventional energetic salts such as ammonium, hydrazinium and hydroxylammonium – which are typically very soluble in water. While reduced solubility can complicate certain processing steps, it also contributes to enhanced safety during handling and storage.

To investigate the influence of cation design on salt stoichiometry and thermal behavior, we prepared both 1:1 (5-Atz based) and 1:2 (dinitroamine based) salts using our newly developed cations with previously reported anions (Fig. 9B and C). This strategy allowed a direct comparison between different coordination modes and cation–anion ratios. In both systems,

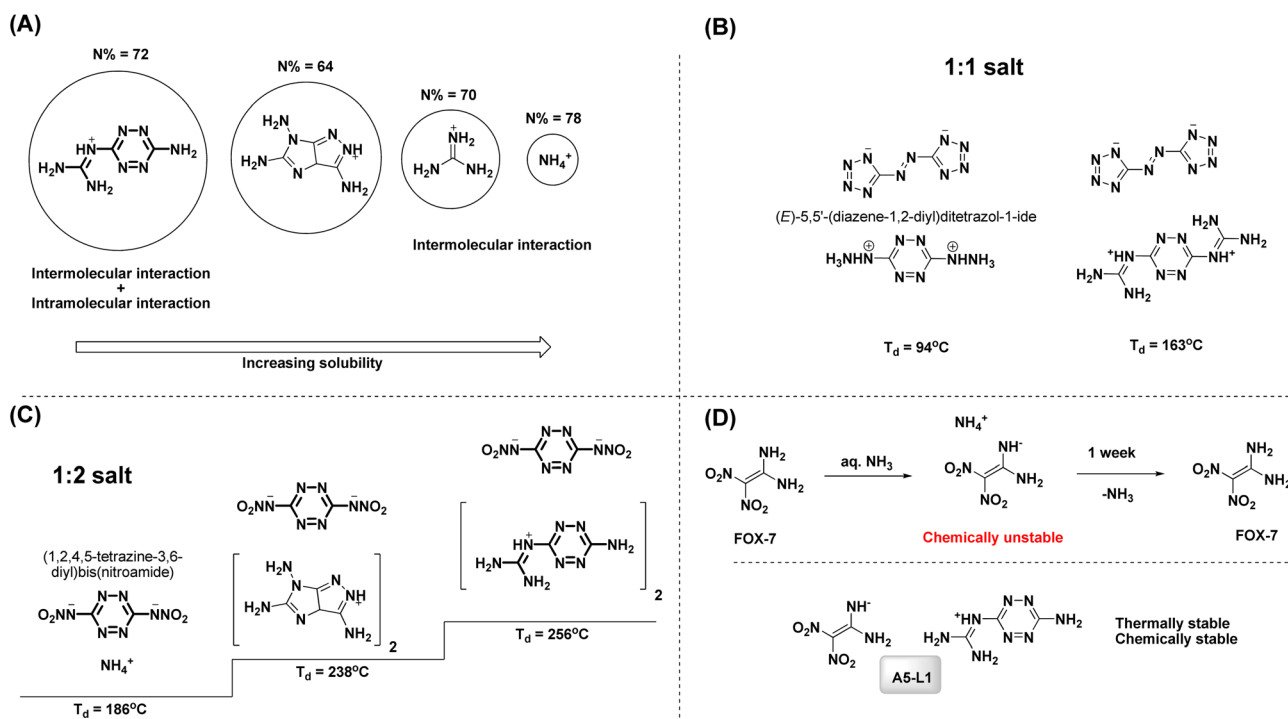


Fig. 9 (A) Size comparison and solubility correlation. (B) Thermal stability comparison of 5-Atz based 1:1 salts. (C) Thermal stability comparison of dinitroamine based 1:2 salts. (D) Stability of FOX-7 energetic salts.



**Table 2** Specific impulse (propulsive properties) for different high energy composite propellant formulations

	$I_{sp}^{a,f}$ [s]	$I_{sp}^{b,f}$ [s]	$I_{sp}^{c,f}$ [s]	$I_{sp}^{d,f}$ [s]	$I_{sp}^{e,f}$ [s]
<b>A1-L1</b>	269	262	251	268	236
<b>A3-2L2</b>	235	240	221	239	229
<b>2</b>	247	253	239	252	232
<b>RDX</b>	267	278	259	268	242

<sup>a</sup>  $I_{sp}$  – Specific impulse of neat compound (monopropellant). <sup>b</sup>  $I_{sp}$  – Specific impulse at 88% compound and 12% Al as fuel additive. <sup>c</sup>  $I_{sp}$  – Specific impulse at 78% compound, 12% Al, and 10% HTPB as a binder. <sup>d</sup>  $I_{sp}$  – Specific impulse at 80% compound, 20% AP. <sup>e</sup>  $I_{sp}$  – Specific impulse at 42% compound, 20% AP, 20% HTPB and 18% Al. <sup>f</sup> Specific impulse calculated at an isobaric pressure of 70 bar and initial temperature of 3300 K using EXPLO5 V 7.01.

the incorporation of the new cations led to a significant increase in thermal stability relative to salts derived from earlier cationic frameworks, highlighting the stabilizing effects of strong stabilizing interactions.

The chemical stability of energetic salts arises from a combination of intrinsic molecular features and extrinsic environmental factors; in our tetrazine-derived salts the dominant stabilizing contributions are structural rather than purely electronic.<sup>57</sup> Intramolecular and intermolecular hydrogen bonding, together with strong  $\pi$ - $\pi$  stacking and compact layer-like packing, restrict molecular mobility and limit access of reactive agents (solvent, moisture, oxygen) to labile sites, thereby increasing resistance to hydrolysis and other chemical degradation pathways. For instance, we have observed that ammonium-FOX slowly reverts to FOX-7 over the period of one week, whereas, the 2:1 and 1:1 salts of FOX-7 anion with L1 and L2 cations make thermally and chemically stable materials with good detonation performance.

To evaluate the applicability of energetic salts **A1-L1**, **A3-2L2**, and zwitterion **2** as solid propellants, their performance was evaluated as monopropellants (neat) and composite propellants. The specific impulse ( $I_{sp}$ ) values were calculated using EXPLO5v7.01.01 software at chamber pressure 7 MPa, expansion pressure ratio ( $P_e/P_c$ ) of 70, initial T of 3300 K, ambient pressure of 0.1 MPa at equilibrium, and expansion through the nozzle. The  $I_{sp}$  values (Table 2) of **A1-L1**, **A3-2L2**. Additionally, the  $I_{sp}$  values of four composite propellant formulations using **A1-L1**, **A3-2L2**, **2** and **RDX** (i) 88% of compound and 12% Al, (ii) 78% of compound, 12% Al, and 10% HTPB. (iii) 80% compound, 20% AP (iv) 42% compound, 20% AP, 20% HTPB and 18% Al, were calculated and the results are given in Table 2. The specific impulse values ( $I_{sp}$ ) of **A1-L1** are comparable to the benchmark explosive RDX.<sup>58–60</sup> **2L2** and **2** as monopropellants (neat) are 269 s, 235 s and 247 s, respectively, which is higher than AP (ammonium perchlorate) (157 s) and ADN (ammonium dinitramide) (206 s).

### 3 Conclusions

In this work, we have designed and synthesized a family of tetrazine-based cations and their salts that integrate high nitrogen content, and facile synthetic accessibility. In addition,

they exhibit remarkable thermal stabilities. Structural analyses reveal planar frameworks stabilized by  $\pi$ - $\pi$  stacking and extensive hydrogen bonding, which contribute to high crystal densities and stability. Thermal analyses demonstrate decomposition temperatures that exceed those of conventional tetrazine derivatives and are comparable to or surpass benchmark energetic materials. The positive heats of formation, together with high detonation velocities and pressures place these tetrazine derivatives among promising candidates for energetic applications. The zwitterion further highlights the versatility of tetrazine scaffolds, combining favorable energetic characteristics with enhanced chemical stability. Overall, cation engineering and zwitterionic design expand the scope of tetrazine chemistry, providing a pathway to thermally robust and high-performing energetic materials.

### Conflicts of interest

The authors declare that they have no competing financial interests or personal relationships that could have influenced the work reported in this paper.

### Data availability

The data underlying this study are available in the published article and its online supporting information (SI). Supplementary information is available. See DOI: <https://doi.org/10.1039/d5ta08126b>.

CCDC 2491019, 2491020 and 2491021 contain the supplementary crystallographic data for this paper.<sup>61a–c</sup>

### Acknowledgements

The diffractometer (Rigaku Synergy S) for SC-XRD was purchased with support from the National Science Foundation (MRI program) under grant no. 1919565. We are grateful to the Fluorine-19 fund for support.

### References

- 1 T. M. Klapötke, *Chemistry of High-Energy Materials*, Walter de Gruyter, 2nd edn, 2012.
- 2 H. Gao, Q. Zhang and J. M. Shreeve, *J. Mater. Chem. A*, 2020, **8**, 4193–4216.
- 3 Z. Xu, T. Hou, F. Yang, L. Zhang, X. Zhang, W. Liu, Q. Lang, M. Lu and Y. Xu, *ACS Appl. Mater. Interfaces*, 2023, **15**, 41580–41589.
- 4 G. Zhang, X. Hao, Y. Zou, S. Liu, J. Wei, Z. Dong and Z. Ye, *J. Mater. Chem. A*, 2024, **12**, 33249–33256.
- 5 D. E. Chavez, D. A. Parrish, L. Mitchell and G. H. Imler, *Angew. Chem. Int. Ed.*, 2017, **56**, 3575–3578.
- 6 T. M. Klapötke, P. C. Schmid, S. Schnell and J. Stierstorfer, *Chem. Eur. J.*, 2015, **21**, 9219–9228.
- 7 T. M. Klapötke, M. Leroux, P. C. Schmid and J. Stierstorfer, *Chem. Eur. J.*, 2016, **11**, 844–851.
- 8 P. Yin, C. He and J. M. Shreeve, *Chem. Eur. J.*, 2016, **22**, 2108–2113.

9 J. Singh, R. J. Staples and J. M. Shreeve, *J. Mater. Chem. A*, 2024, **12**, 30548–30557.

10 J. Singh, R. J. Staples and J. M. Shreeve, *J. Mater. Chem. A*, 2023, **11**, 12896–12901.

11 M. Benz, T. M. Klapotke, J. Stierstorfer and M. Voggenreiter, *J. Am. Chem. Soc.*, 2022, **144**, 6143–6147.

12 Q. Yu, Z. Zheng, Z. Yi, W. Yi and J. M. Shreeve, *J. Am. Chem. Soc.*, 2025, **147**, 5125–5131.

13 J. Singh, R. J. Staples and J. M. Shreeve, *Sci. Adv.*, 2023, **9**, eadk3754.

14 D. Fischer, T. M. Klapötke, J. Stierstorfer and N. Szimhardt, *Chem. Eur. J.*, 2016, **22**, 4966–4970.

15 X. Yu, J. Tang, C. Lei, C. Xue, G. Cheng, C. Xiao and H. Yang, *J. Mater. Chem. A*, 2024, **12**, 19513–19520.

16 B. Tan, J. Su, J. Zhang, C. Tang, J. Dou, X. Yang, M. Xu, S. Zeng, W. Li, J. Luan, G. Zhang, S. Song, Q. Zhang, X. Lu, B. Wang and N. Liu, *J. Mater. Chem. A*, 2025, **13**, 25103–25109.

17 X. Guo, Y. Feng, Y. Liu, Q. Liu, L. Q. Luo and H. Gao, *J. Mater. Chem. A*, 2025, **13**, 10782–10791.

18 R. Lv, L. Jiang, J. Wang, S. Huang, S. Song, L. Wei, Q. Zhang and K. Wang, *J. Mater. Chem. A*, 2024, **12**, 10050–10058.

19 P. Saini, J. Singh, R. J. Staples and J. M. Shreeve, *J. Mater. Chem. A*, 2025, **13**, 17421–17428.

20 W. Hu, J. Tang, X. Ju, Z. Yi, H. Yang, C. Xiao and G. Cheng, *ACS Cent. Sci.*, 2023, **9**, 742–747.

21 N. Fischer, D. Fischer, T. M. Klapötke, D. G. Piercy and J. Stierstorfer, *J. Mater. Chem.*, 2012, **22**, 20418.

22 S. Banik, P. Kumar, V. D. Ghule, S. Khanna, D. Allimuthu and S. Dharavath, *J. Mater. Chem. A*, 2022, **10**, 22803–22811.

23 P. Bhatia, K. Pandey, B. Avasthi, P. Das, V. D. Ghule and D. Kumar, *J. Org. Chem.*, 2023, **88**, 15085–15096.

24 J. Singh, R. J. Staples, M. Fabin and J. M. Shreeve, *J. Mater. Chem. A*, 2024, **12**, 17501–17509.

25 P. Bhatia, P. Das and D. Kumar, *ACS Appl. Mater. Interfaces*, 2024, **16**, 64846–64857.

26 H. Gao and J. M. Shreeve, *Chem. Rev.*, 2011, **111**, 7377–7436.

27 W. Liu, W. L. Liu and S. P. Pang, *RSC Adv.*, 2017, **7**, 3617–3627.

28 K. Pandey, P. Das, A. Bijlwan and D. Kumar, *J. Org. Chem.*, 2025, **90**, 7700–7711.

29 D. Kumar and A. J. Elias, *Resonance*, 2019, **24**, 1253–1271.

30 M. Benz, T. M. Klapötke, J. Stierstorfer and M. Voggenreiter, *ACS Appl. Eng. Mater.*, 2022, **1**, 3–6.

31 D. E. Chavez, M. A. Hiskey and R. D. Gilardi, *Org. Lett.*, 2004, **6**, 2889–2891.

32 M. H. V. Huynh, M. A. Hiskey, D. E. Chavez, D. L. Naud and R. D. Gilardi, *J. Am. Chem. Soc.*, 2005, **127**, 12537–12543.

33 D. E. Chavez, B. C. Tappan, M. A. Hiskey, S. F. Son, H. Harry, D. Montoya and S. Hagelberg, *Propellants, Explos. Pyrotech.*, 2005, **30**, 412–417.

34 D. E. Chavez and M. A. Hiskey, *J. Heterocycl. Chem.*, 1998, **35**, 1329–1332.

35 Q. Yu, J. Singh, R. J. Staples and J. M. Shreeve, *Chem. Eng. J.*, 2022, **431**, 133235.

36 X. Zhang, Y. Wang, Y. Liu, Q. Zhang, L. Hu, C. He and S. Pang, *ACS Appl. Mater. Interfaces*, 2022, **14**, 37975–37981.

37 D. M. Bystrov, A. N. Pivkina and L. L. Fershtat, *Molecules*, 2022, **27**, 5891.

38 H. Zhang, X. Du, Y. Liu, G. Lei, P. Yin and S. Pang, *ACS Omega*, 2024, **9**, 33557–33562.

39 W. Tu, L. Wen, K. Wang, Y. Liu and Z. Xie, *J. Org. Chem.*, 2025, **90**, 7766–7774.

40 L. L. Fershtat, *FirePhysChem*, 2023, **3**, 78–87.

41 M. D. Coburn, G. A. Buntain, B. W. Harris, M. A. Hiskey, K. -Y Lee and D. G. Ott, *J. Heterocycl. Chem.*, 1991, **28**, 2049–2050.

42 G. F. Rudakov, T. V. Ustinova, I. B. Kozlov and V. F. Zhilin, *Chem. Heterocycl. Compd.*, 2014, **50**, 53–64.

43 N. Fischer, K. Hüll, T. M. Klapötke, J. Stierstorfer, G. Laus, M. Hummel, C. Froschauer, K. Wurst and H. Schottenberger, *Dalt. Trans.*, 2012, **41**, 11201–11211.

44 A. J. Paraskos, E. D. Cooke and K. C. Caflin, *Propellants, Explos. Pyrotech.*, 2015, **40**, 46–49.

45 D. E. Chavez and M. A. Hiskey, *J. Energ. Mater.*, 1999, **17**, 357–377.

46 H. Gao, R. Wang, B. Twamley, M. A. Hiskey and J. M. Shreeve, *Chem. Commun.*, 2006, **4007**, 4007–4009.

47 M. Anniyappan, M. B. Talawar, G. M. Gore, S. Venugopalan and B. R. Gandhe, *J. Hazard. Mater.*, 2006, **137**, 812–819.

48 Q. Yu, P. Yin, J. Zhang, C. He, G. H. Imler, D. A. Parrish and J. M. Shreeve, *J. Am. Chem. Soc.*, 2017, **139**, 8816–8819.

49 M. A. Spackman and J. J. McKinnon, *CrystEngComm*, 2002, **4**, 378–392.

50 M. A. Spackman and D. Jayatilaka, *CrystEngComm*, 2009, **11**, 19–32.

51 NATO, Standardization Agreement 4489 (STANAG4489), Explosives, Impact Sensitivity Tests, 1999.

52 NATO, Standardization Agreement 4487 (STANAG 4487), Explosives, Friction Sensitivity Tests, 2002.

53 M. J. Frisch, G. W. Trucks, H. B. Schlegel and G. E. Scuseria, *et al.*, *Revision D.01*, Gaussian Inc., Wallingford CT, 2003 Search PubMed.

54 M. Sućeska, *EXPLO5, Version 7.01.01*, Brodarski Institute, 2019 Search PubMed.

55 R. Mayer, J. Köhler and A. Homburg, *Explosives*, Wiley-VCH, 2007.

56 C. B. Storm, J. R. Stine and J. F. Kramer, *Chem. Phys. Energ. Mater.*, 1990, 605–639.

57 D. Herweyer, A. A. Kitos, P. Richardson, H. Canoe, J. S. Ovens, I. Laroche, B. Jolicoeur, M. Murugesu and J. L. Brusso, *Cryst. Growth Des.*, 2023, **23**, 2576–2582.

58 M. Tang, X. Wang, X. Xu, Z. Zeng, C. Chen, Y. Liu, W. Huang and Y. Tang, *J. Mater. Chem. A*, 2024, **12**, 13081–13085.

59 T. M. Klapötke, *Chemistry of High-Energy Materials*, De Gruyter, edn. 6, 2022.

60 D. Luca, *Chemical Rocket Propulsion*, Springer Aerospace Technology, 2017.

61 (a) CCDC 2491019: ExperimentalCrystal Structure Determination, 2025, DOI: [10.5517/ccdc.csd.cc2pm3gx](https://doi.org/10.5517/ccdc.csd.cc2pm3gx); (b) CCDC 2491020: ExperimentalCrystal Structure Determination, 2025, DOI: [10.5517/ccdc.csd.cc2pm3hy](https://doi.org/10.5517/ccdc.csd.cc2pm3hy); (c) CCDC 2491021: ExperimentalCrystal Structure Determination, 2025, DOI: [10.5517/ccdc.csd.cc2pm3jz](https://doi.org/10.5517/ccdc.csd.cc2pm3jz).

